Eur. Phys. J. Plus (2022) 137:1243
https://doi.org/10.1140/epjp/s13360-022-03454-4

THE EUROPEAN PHYSICAL JOURNAL PLUS

Regular Article

The structural, elastic, electromagnetic and optical response of quaternary Heusler CoFeTiZ (Z = Ge, Sb) alloys: a DFT study with mBJ and mBJ + SOC methods

Muhammad Jamil[1], **Quratul Ain**[2], **Moeen Ud Din**[1], **Masood Yousaf**[3], **Junaid Munir**[1,a]

[1] Department of Physics, Riphah International University, Lahore, Pakistan
[2] Department of Physics, University of Management and Technology, Lahore, Pakistan
[3] Department of Physics, University of Education, Lahore, Pakistan

Received: 8 July 2022 / Accepted: 2 November 2022

Abstract The spin–orbit coupling effect and the modified Becke-Johnson potential have been employed to calculate the ground-state response of quaternary Heusler CoFeTiZ (Z = Ge, Sb) alloys. For this purpose, we use the full-potential linearized augmented plane wave method along with the spin-polarized calculations implemented in WIEN2k simulation code. The optimization curves and the negative formation energies of both alloys confirm their stable structures. The mechanical stability is achieved through the calculation of the elastic parameters. A metallic nature is observed in the spin-up states. The spin-dn states show a semiconductor behavior with energy gap values of 0.842 and 0.949 eV for CoFeTiGe and 0.772 and 0.809 eV for CoFeTiSb with mBJ and mBJ + SOC, respectively. The contribution of Co and Fe atoms is dominant to the overall magnetic behavior of alloys. The optical response is evaluated through several optical parameters. The maximum absorption is observed in the visible region for both alloys. The calculated properties reveal the potential of studied alloys for spintronic and optoelectronic applications.

1 Introduction

The coexistence of electronic charge and spin makes the spintronic devices more special than regular electronic devices [1]. Half-metallic ferromagnetic (HMF) compounds have 100% spin-polarization (SP) with the electron states present at the Fermi level. Heusler alloys are particularly remarkable among HMFs because of their high spin-polarization (SP) and tunable electronic structure [2, 3]. Heusler alloys are important because of their novel functions and significant prospective uses in spintronics [4–6]. Spintronics is a fast-growing field concerned with the transportation of the spin-polarized electrons [7]. Electrons travel quicker in totally spin-polarized materials than in typical semiconducting materials and nonpolar compounds. The strongly spin-polarized charge carriers in HM materials make them a feasible candidate for spintronic devices [8]. Spintronic-based devices have large data storage capacity, faster data processing and a faster data transmission rate [9–11]. Recently, Heusler alloys have been extensively studied theoretically and experimentally [12–17]. A novel class of Heusler alloys, notably the equiatomic quaternary Heusler alloys (EQHA), shows a lot of interest due to their distinctive and exciting properties, such as high spin-polarization and spin gapless semiconductor (SGS) [18–21]. Several researchers have recently become interested in Heusler alloys, particularly the equiatomic quaternary Heusler. The characteristics of CoMnCrSb have been theoretically described in the literature by Saadi Berri et. al. [22]. Several other equiatomic quaternary Heusler alloys (EQHAs), like CoFeScZ (Z = Sb, P, As) [4], CoMnTiZ (Z = Sb, P, As,) [23–26] CoRhMnZ(Z = Al, Ga, Ge, Si) [27] and CoFeMnZ(Z = As, Si, Sb) [23], have been intensively discussed in the literature. Recently, quaternary half-metallic Heusler alloys CoFeTiSn and CoFeTiGa$_{1-x}$Sb$_x$ have been investigated deeply to understand their electromagnetic properties [28, 29]. The structural formula for full-Heusler alloys is X_2YZ having $L2_1$ structure and half Heusler alloy is XYZ having $C1_b$ structure, where X and Y are transition metals and Z is a main-group element. One more class is the quaternary Heusler alloys (QHAs) with the formula XX′YZ. Certain theoretical studies, particularly in Co-based alloys with the $L2_1$ structure predicted the HM behavior in Heusler compounds [30–36]. The fascinating properties of Heusler alloys have attracted researchers, and they have studied a large number of QHAs as presented in the literature. These alloys motivated and inspired the research community due to their demand in industry and the digital world to explore new potential quaternary Heusler alloys. We have studied the new quaternary Heusler alloys CoFeTiGe, and CoFeTiSb in the present research work. The previous work done on these alloys not only underestimated the bandgap values but also did not include the spin–orbit coupling effect, which is an important parameter in determining the accurate properties of magnetic materials. Various properties such as structural, elastic, electromagnetic and optical properties are investigated using different potentials implemented via WIEN2k code.

[a] e-mail: junaid_ij2000@yahoo.com (corresponding author)

Published online: 15 November 2022

2 Computational methodology

The first principle method, along with the spin-polarized calculations, is used to determine the physical properties of CoFeTiZ (Z = Ge, Sb) alloys. The density-functional theory-based calculations are performed using the full-potential linearized augmented plane wave (FP-LAPW) approach implemented in the WIEN2k computational code [37]. The electrical structure of the compounds can be calculated using the well-known Kohn–Sham (KS) equations.

$$\left(-\frac{1}{2}\nabla^2 + \upsilon_{\mathrm{eff},\sigma}^{\mathrm{K-S}}(\boldsymbol{r})\right)\psi_{i,\sigma}(\boldsymbol{r}) = \in_{i,\sigma}\ \psi_{i,\sigma}(\boldsymbol{r}) \tag{1}$$

where $\nu_{\mathrm{eff},\sigma}^{\mathrm{K-S}} = V_{\mathrm{ext}}+V_{\mathrm{H}}+V_{xc,\sigma}$ is the Kohn–Sham's external potential, and it is the sum of external, Hartree, and exchange–correlation (xc) terms. $\psi_{i,\sigma}$ is the one-electron wave function [38]. The mBJ scheme is applied to investigate the electronic properties, anticipating good results for band structure in semiconductors, particularly for half-metallic (HFs) ferromagnetism [39]. The modified Becke Johnson expresses as [40].

$$\upsilon_x^{\mathrm{mBJ}}(r) = c\upsilon_x^{\mathrm{Br}}(\boldsymbol{r}) + (3(-2))\frac{1}{\pi}\sqrt{\frac{5}{12}}\sqrt{\frac{2t(r)}{\rho(r)}} \tag{2}$$

where $\nu_x^{\mathrm{mBJ}}(r)$ represents the Becke–Roussel (BR) potential, c is the system-dependent parameter linked with BJ potential and its equal to unity which can be found by the following empirical relation.

$$c = \alpha + \beta\left(\frac{1}{V_{\mathrm{cell}}}\int_{V\mathrm{cell}}\frac{\nabla\rho(r)}{\rho(r)}\right)^{\frac{1}{2}} \tag{3}$$

V_{cell} is the unit cell volume. The α and β are used to fit the bandgap.

The spin–orbit coupling (SOC) effect must be significant in the materials containing heavy metals. We have included the SOC in our computation using the second variational technique [41], and the Hamiltonian can be expressed with the following relation:

$$H = -\frac{\hbar}{2m}\nabla^2 + V_{\mathrm{eff}} + H_{\mathrm{SO}} \tag{4}$$

H_{SO} is known spin–orbit coupling defined as:

$$H_{\mathrm{SO}} = \frac{1}{2Mc^2}\frac{1}{r^2}\frac{\mathrm{d}v_{MT}}{\mathrm{d}r}\begin{pmatrix}\vec{\sigma}\cdot\vec{1} & 0\\ 0 & 0\end{pmatrix} \tag{5}$$

$\vec{\sigma}$ Pauli spin matrix.

During the calculations, the spherical harmonics expansion is limited to $l_{\max} = 10$, and the plane waves are set up to $R_{\mathrm{MT}}K_{\max} = 7$. The reduced muffin-tin radii (RMT) (a.u) of the individual atoms are Co = 2.3, Fe = 2.3, Ti = 2.19, and Ge = 2.19 for CoFeTiGe and Co = 2.29, Fe = 2.35, Ti = 2.35 and Sb = 2.35 for CoFeTiSb. For the upper limit expansion of the potential and charge, $G_{\max} = 24$ a u^{-1} is chosen. The energy cutoff −9.0 Ryd separates the valence and core states. A number of K-points 1300 are used to get the results with great accuracy in the first Brillouin zone. The energy convergence is improved to 10^{-4} [Ry] by involving the iteration procedure.

3 Results and discussion

3.1 Structural stability

The quaternary Heusler alloys (QHAs), having general formula XX′YZ with the space group F$\bar{4}$3m, are investigated. The unit cell consists of four formula units occupying four Wyckoff positions: 4a (0; 0; 0), 4b (0.25; 0.25; 0.25), 4c (0.5; 0.5; 0.5) and 4d (0.75; 0.75; 0.75). First, we optimize the crystal structures to find the ground-state lattice parameters. Structure optimization graphs of both alloys are shown in Fig. 1.

The structures are optimized in both non-magnetic (NM) and ferromagnetic (FM) states to check the most stable state. The lowest ground-state energy is achieved in the FM state, making it more stable than the NM state, and depicted from the optimization curves. Birch–Murnaghan equation of state (EOS) [42] is utilized to calculate the lattice constants which represented as:

$$E(V) = E_0 + \frac{B_0V_0}{16}\left\{\left[\left(\frac{V_0}{V}\right)^{\frac{2}{3}} - 1\right]B_0' + \left[\left(\frac{V_0}{V}\right)^{\frac{2}{3}} - 1\right]\left[6 - 4\left(\frac{V_0}{V}\right)^{\frac{2}{3}} - 1\right]\right\} \tag{6}$$

Here E_0 is the minimum ground-state energy achieved during the optimization, unit cell volume is V and equilibrium volume is V_0. B_0 is the Bulk modulus and its derivative is presented with B'. The stability of the studied alloys is further confirmed with the

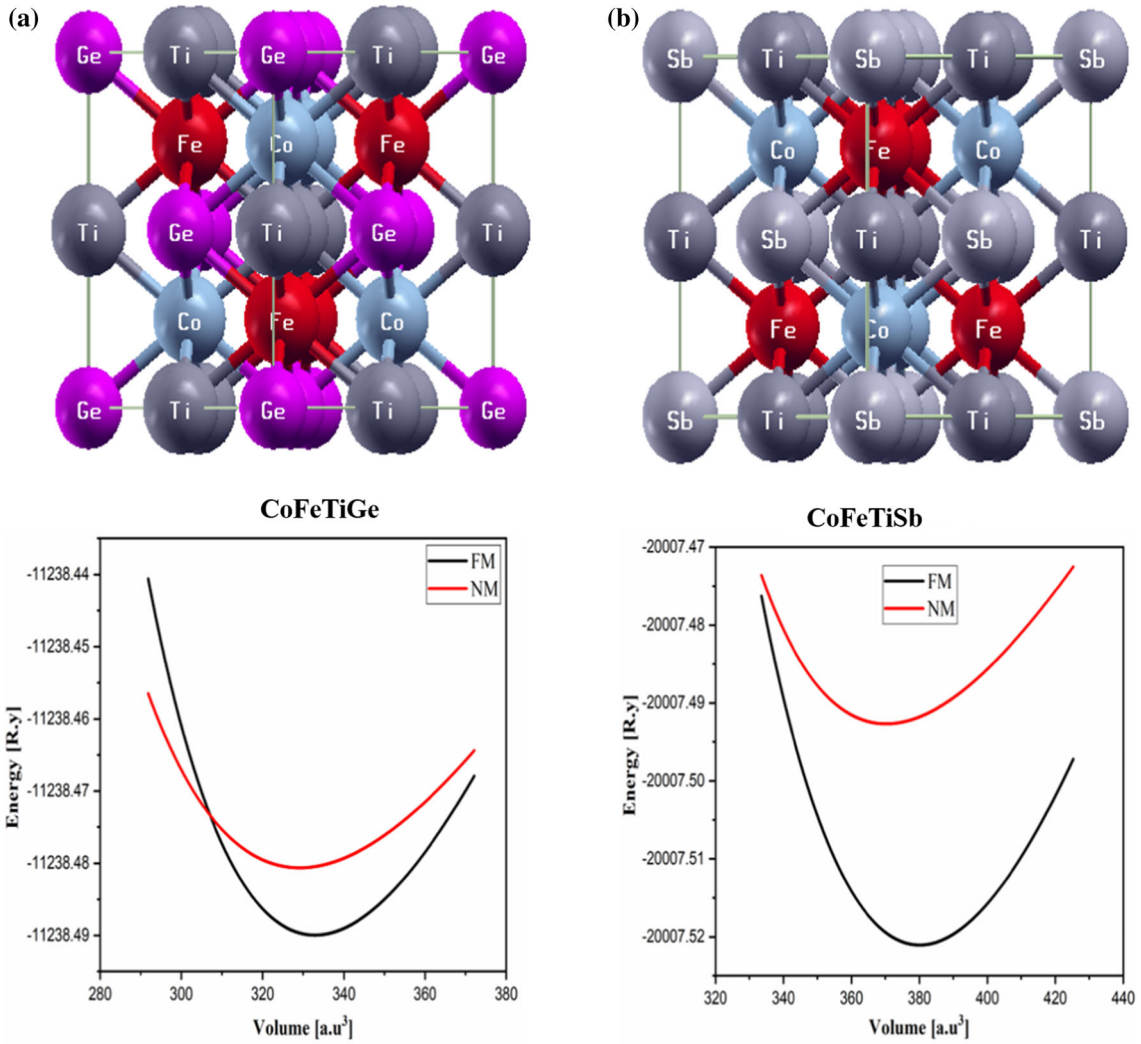

Fig. 1 Crystal structure and optimization curve in **a** CoFeTiGe and **b** CoFeTiSb for both QHAs, respectively

Table 1 Calculated lattice parameters of CoFeTiZ (Z = Ge, Sb) alloys

Lattice parameters $a\left(A^0\right)$			Bulk modulus B (GPa)		B'	V_o	E_0(Ry)	Formation energy
	Our work	Other work	Our work	Other work	Our work	Our work	Our work	Our work
CoFeTiGe	5.81	5.8	207.31		11.98	331.32	− 11,238.4886	− 1.69 eV/atom
CoFeTiSb	6.08	–	195.15	–	5.98	379.99	− 20,007.5210	− 1.55 eV/atom

formation energy. Formation energy is basically the difference in energy between the bulk material and its individual elements. It can be found by using the following relation:

$$E_F = E_{(CoFeTiZ\ (Z=Ge,Sb))} - E_{(Co)} - E_{(Fe)} - E_{(Ti)} - E_{(Z)} \tag{7}$$

Here, $E_{(CoFeTiZ\ (Z=Ge,\ Sb))}$ is the total energy of the alloys and the subsequent terms show the individual energies of each atom. The negative values of formation energy are achieved for both alloys, which means that the cubic phases of the alloys can be easily synthesized. The elastic parameters are presented in Table 1.

Table 2 Calculated mechanical parameters of CoFeTiZ (Z = Ge, Sb) alloys

Alloys	C_{11}	C_{12}	C_{44}	G	B	Y	B/G	υ	A
CoFeTiGe	320.89	170.98	73.31	88.27	208.27	203.23	2.78	0.35	0.8
Other work	328.45	138.62	71.10	74.05	201.89	197.81	2.72	0.34	0.8
CoFeTiSb	290.73	162.81	73.39	82.88	197.54	191.89	4.09	0.38	1.0
Other work	–	–	–	–	–	–	–	–	–

4 Elastic properties

Elastic properties are investigated to check the mechanical stability of the alloys. The ability of a material to retain its original shape after removing the stress is called elasticity. The elastic parameters of solids are related to technological applications, such as thermoelastic stress, load deflection, sound velocities, fracture toughness on elastic qualities and internal strain [43]. These properties can provide critical information on the forces acting on solids and materials' phase stability and stiffness. There are three independent elastic constants C_{11}, C_{12} and C_{44} for the cubic symmetry. These elastic constants provide information related to the stability and stiffness of the materials. C_{11} identifies the longitudinal deformation while C_{12} measures the compound's transverse expansion, and C_{44} identifies the shape elasticity. Mechanical parameters such as anisotropy ratio (A), Young's modulus (Y), bulk modulus (B), shear modulus (G) and elastic constants C_{11}, C_{22}, and C_{44} are calculated. These parameters are presented in Table 2.

The shear modulus (G) of a compound can be used to figure out its hardness more accurately. G and B provide information about the resistance to plastic deformation and resistance to fracture, respectively. The results of G and B illustrate the compressibility and stiffness of materials as given by the following relations [44].

$$B = \frac{C_{11}C_{12}}{3} \tag{8}$$

$$G = \frac{G_{\mathrm{V}} + G_{\mathrm{R}}}{2} \tag{9}$$

$$C_{\mathrm{V}} = \frac{C_{11} - C_{12} + 3C_{44}}{5} \tag{10}$$

$$G_{\mathrm{R}} = \frac{5C_{44}(C_{11} - C_{12})}{4C_{44} + 3(C_{11} - C_{12})} \tag{11}$$

where G_{R} and G_{V} express the Reuss shear modulus and Voigt.

Pugh's ratio (B/G) is the most helpful criterion for predicting material nature. The calculated Pugh's ratio falls in criteria [34]; according to this, if $\frac{B}{G} > 1.75$, the material nature becomes ductile; other than, the material behaves brittle. It is clear from the results in Table 4 that $\frac{B}{G} > 1.75$, which indicates that both alloys have ductile characteristics. Poisson's ratio (υ) is another elastic parameter that measures compressibility.

$$\upsilon = \frac{3B - 2G}{2(3B + G)} \tag{12}$$

Most Heusler alloys have Poisson's ratio in the range of 0.2–0.49. In our case, the values of υ for both studied alloys are suitable for this range, as predicted in Table 2. It is clear from the table that the calculated Poisson's ratio for both alloys are 0.32 and 0.38, respectively, which shows that these alloys are stable against external deformation and less compressible. Furthermore, Poisson's ratio provides extra information about the bonding forces' properties [45]. Anisotropy factor (A) is investigated by applying these elastic parameters as,

$$A = \frac{2C_{44}}{C_{11} - C_{12}} \tag{13}$$

Young's modulus Y by,

$$Y = \frac{9BG}{3B + G} \tag{14}$$

From the results, it is clear that the results satisfy the generalized stability criteria. This proved that the compound is mechanically stable.

Spin-polarized contour plots of electron density along (110) planes are used to calculate the bonding nature of the atoms in the alloys, as shown in Fig. 2.

Figure 2a shows the localized charge distribution between Co and Fe atoms in both spin-up and spin-dn states and hence confirms the ionic bonding. A weak covalent bonding can be seen between Ti and Ge atoms. In the case of CoFeTiSb, Co and Fe show ionic bonding, while Ti and Ge possess week covalent bonds in spin-up states. In spin-dn states, all atoms show weak covalent bonding. The mixed nature of bonding (both ionic and covalent) is observed in both alloys. The change in the shape of Co and Fe (Spin-up) from spherical to (Spin-dn) dumbbell for both alloys is due to the electronic transition from filled to partially filled d-bands.

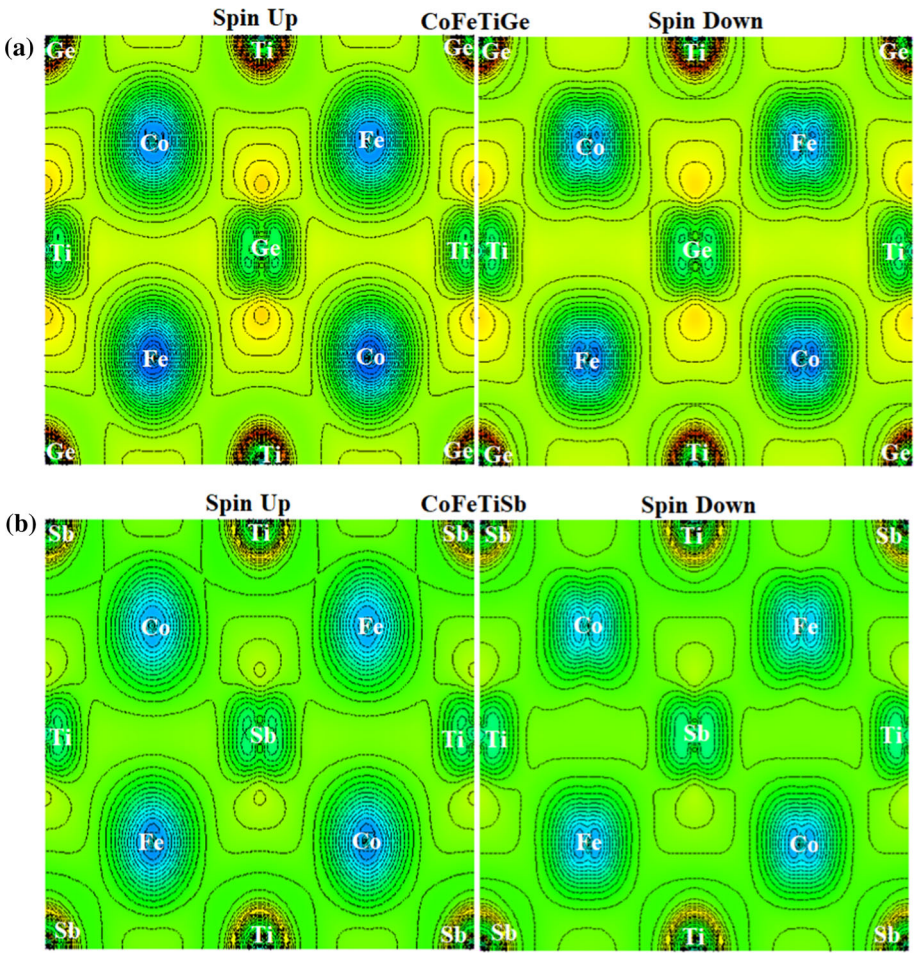

Fig. 2 Contour plots of electron density along (110) plane of **a** CoFeTiGe and **b** CoFeTiSb alloys

5 Electronic properties

Electronic properties play a crucial role in reporting compounds' half-metallic response and play a significant part in understanding the material's efficiency for spintronic/memory/smart devices in modern technology. The band structure, total and partial densities of states are essential to elaborate the electronic nature of the compounds. The optimized lattice parameters are used to simulate the spin-polarized band structures of the selected alloys CoFeTiZ (Z = Ge, Sb) in both majority (↑) and minority (↓) spin states with mBJ and mBJ + SOC potentials and are presented in Fig. 3. The energy bands illustrate the achievable energy of an electron as a wave vector function. As a result, reciprocal space is used to symbolize these bands. The minimum difference between the lowest energy of the conduction bands of minority and majority spin states with respect to Fermi level (E_F), and the absolute value of the highest energy of the valence band of minority and majority spin states causes the half-metallic bandgap (E_{HM}) [46, 47]. In terms of high symmetry directions, Fig. 3 displays the band structure in the first Brillouin zone associated with the ground state [48, 49]. It is shown that the majority (↑) spin states possess a metallic character and minority (↓) spin states show a semiconducting nature for both alloys with the respective potentials. In the case of CoFeTiGe, the maxima of the valence band lie at − 0.016 eV and the minima of the conduction band at 0.826 eV resulting in an energy gap of 0.842 eV around the Fermi level for the minority (↓) spin states with mBJ potential. An improvement in the bandgap, i.e., 0.949 eV is achieved with mBJ + SOC potential. For CoFeTiSb, the obtained bandgap in the minority (↓) spin states is 0.772 eV with mBJ while introducing the SOC enhanced its value up to 0.809 eV. The comparison of the calculated bandgap values with the available literature is given in Table 3. It can be seen that the computed bandgap values in our work are higher and more accurate than the already studied values.

The existence of the bandgap conduces the full spin-polarization at the Fermi level and endorses the half-metallic nature of both alloys. The materials with half-metallic characteristics are also called the spin-flip gap materials and the half-metallic nature measures the mandatory energy to transfer spin-dn states (↓) electrons to the Fermi level of spin-up states (↑) electrons. Practically those compounds have significant utility in modern applications.

The number of electronic states per unit energy is known as the density of states (DOS) and the Fermi level is used as a reference point to describe the DOS. The density of states is an essential parameter to deeply understand the electronic properties of the material. Figure 4 shows the total density of states (TDOS) as a function of energy. A half-metallic nature is observed for both alloys

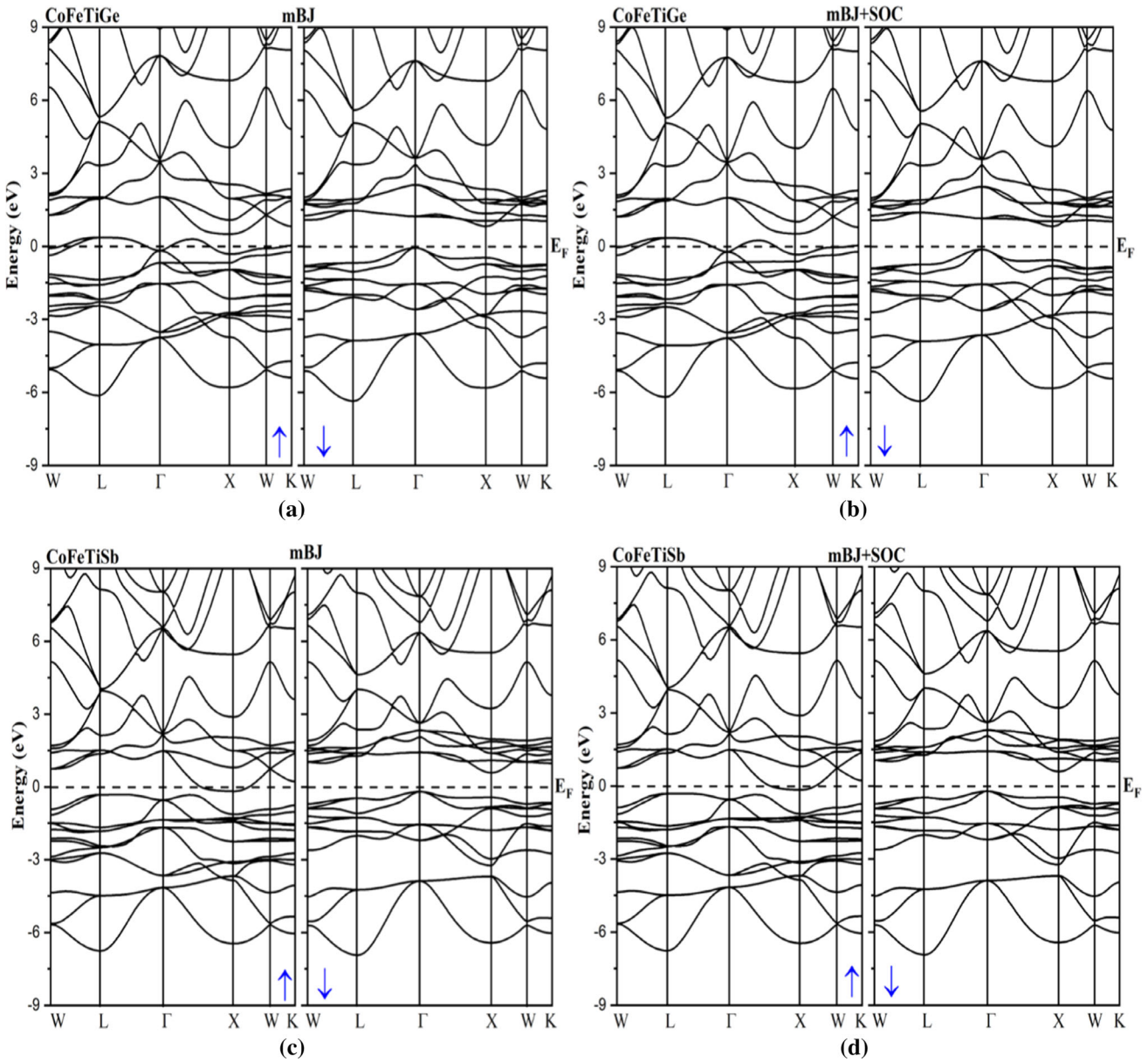

Fig. 3 Calculated band structure of CoFeTiGe (**a**, **b**) and CoFeTiSb (**c**, **d**) alloys with mBJ and mBJ + SOC potentials

Table 3 Calculated bandgap of CoFeTiGe and CoFeTiSb with mBJ and mBJ + SOC potential

E_g (ev)			
Alloys	Our work		Other work
	mBJ	mBJ + SOC	
CoFeTiGe	0.842	0.949	0.383[50], 0.424[51], 0.489[52], 0.07[53]
CoFeTiSb	0.772	0.809	0.53[54], 0.02[53], 0.13[55]

which is the confirmation of the band structure profile results. The detailed interpretation of the individual contribution of dissimilar states of different atoms can be presented with the partial density of states (PDOS). Galanakis et al. [56] show the link between hybridization and the origin of the energy gap. The origin of the minority bandgap (↓), including the orbital hybridization of both alloys can be explained on the basis of classical molecular orbital approach. The orbital hybridization of *d*-states of Ti, Fe, and Co atoms is only considered because the *sp*-bands are situated at deep energy and make a contribution to the top. The *d*-orbitals of Fe and Co split into doubly degenerate e_g $\left(d_z^2, d_{x^2-y^2}\right)$ and triply degenerate t_{2g} $\left(d_{xy}, d_{yz}, d_{zx}\right)$ orbitals. Double degenerate orbitals at Co site can only couple with double degenerate orbitals at the other Co site or at the Fe site [56].

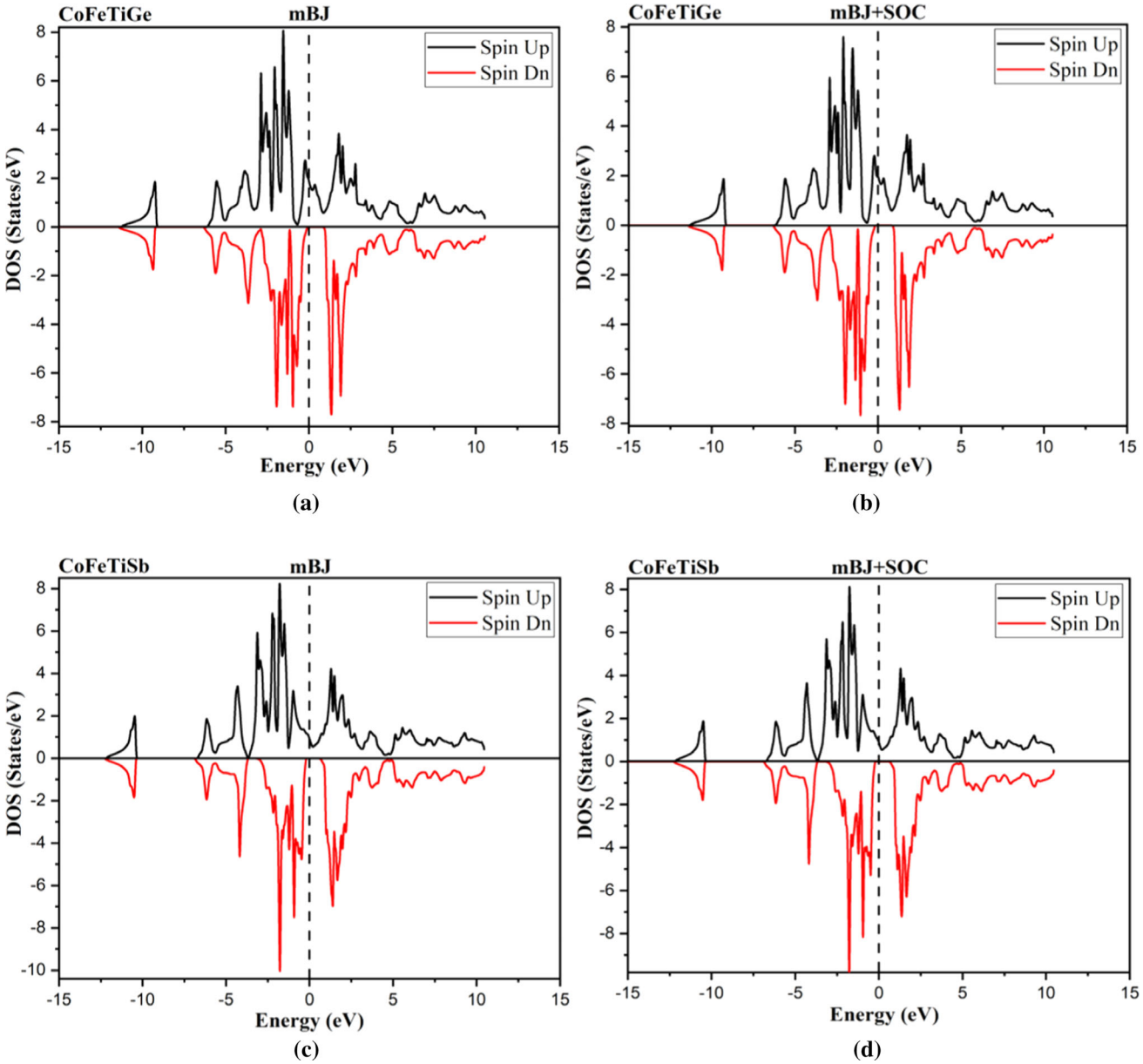

Fig. 4 The calculated total spin-polarized density of state for CoFeTiZ (Z = Ge, Sb) compounds with mBJ and mBJ + SOC potentials

The extraction of the half-metallic characteristics of CoFeTiZ (Z = Ge, Sb) alloys can be done by introducing the conceivable hybridization between the ingredient atoms schematically. The $d-d$ hybridization in transition metals causes the bandgap generation in the minority spin (↓) states and, as a result, the half-metallic character in the QHAs alloys.

To demonstrate the individual contribution of each element, the partial density of states (PDOS) is computed and presented in Fig. 5. The t_{2g} states show the main contribution in the valence band for spin-up and spin-dn states, while their contribution is smaller in the conduction band with both potentials. A noticeable contribution of e_g states is observed in the valence band for both spin states with mBJ and mBJ + SOC potentials. The maximum contribution of e_g states can be seen in the spin-dn states of the conduction band with both potentials. The contribution of the other states is negligibly small, so they are not included in the figure.

The magnetic properties of the selected quaternary Heusler alloys are also investigated. The individual and total magnetic moment of CoFeTiZ (Z = Ge, Sb) alloys are summarized in Table 4.

The calculated magnetic moment of Co and Fe is positive, which shows FM coupling among Co and Fe. The Ge and Sb have a negative values, which is due to the induced magnetic polarization of these elements that is antiparallel with Co and Fe atoms.

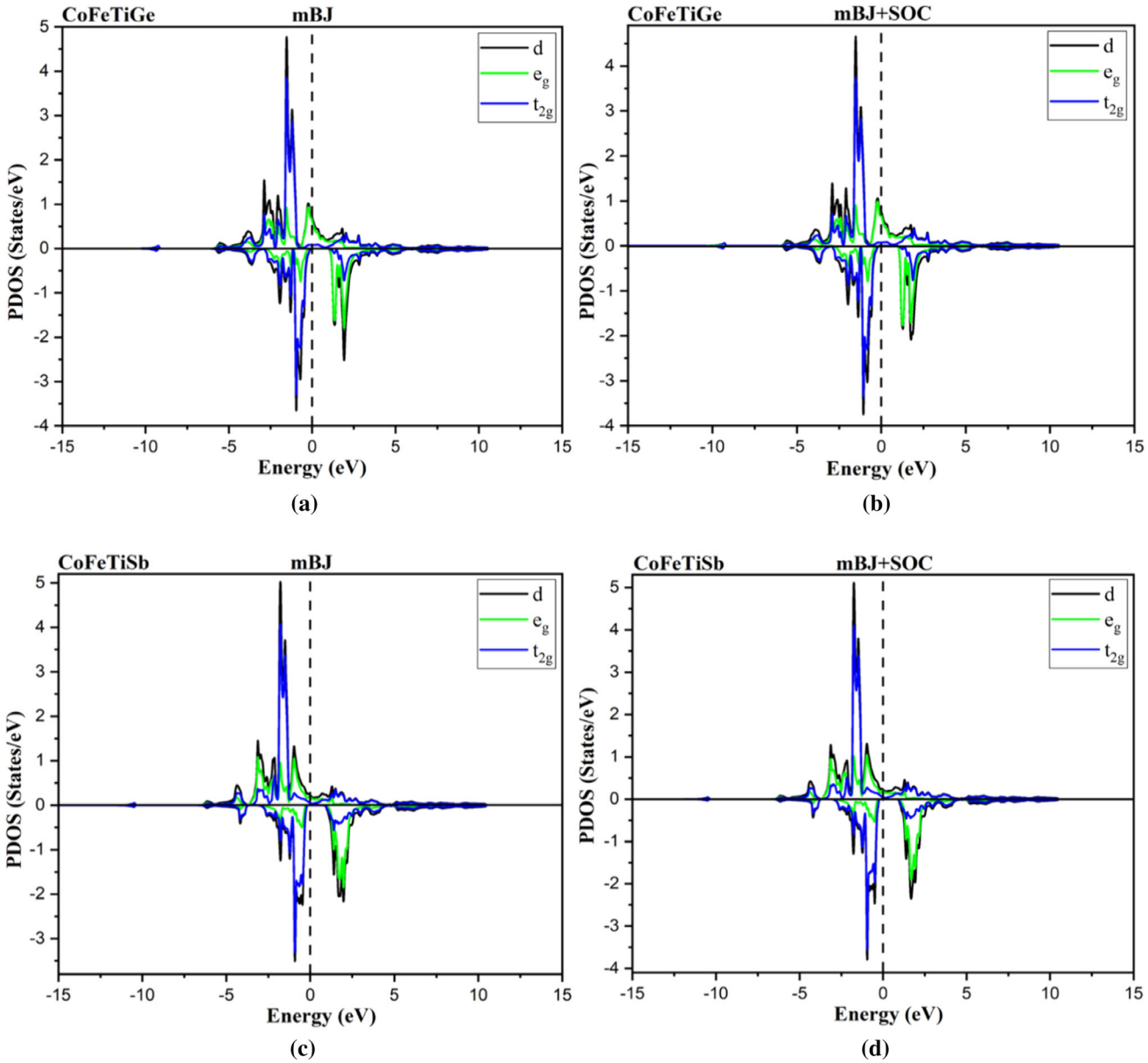

Fig. 5 Calculated spin-polarized partial density of states for CoFeTiZ (Z = Ge, Sb) with mBJ and mBJ + SOC potentials

6 Optical properties

The optical properties are significant for assessing the material's behavior in the presence of incident electromagnetic waves [59]. The optical parameters are essential to find the efficient applications of the materials for optoelectronics and photovoltaic devices. One of the most important parameters, i.e., optical conductivity, is associated with the dielectric constant. Optical conductivity is the electrical conductivity due to the electric field. The optical term is not only associated with the visible region but also covers the entire frequency range of the spectrum. The Drude model well explains the optical parameters [60]. The optical properties of CoFeTiZ (Z = Ge, Sb) alloys are calculated to examine their optical response. The first thing is to understand the complex dielectric function $\varepsilon(\omega) = \varepsilon_1(\omega) + \iota\varepsilon_2(\omega)$, where the imaginary component $\varepsilon_2(\omega)$, is calculated using the following formula from the electronic band structure [61].

$$\varepsilon_2(\omega) = \frac{V_e^2}{m^2\omega^2}\int d^3k\Sigma_{nm'}\left|\overrightarrow{<\vec{k}n}\left|p\right|\vec{k}n'>\right|^2\left(\vec{k}n\right)\left[1 - f\left(\left(\vec{k}n'\right)\right]E_{\vec{k}n} - E_{\vec{k}n'} - \hbar\omega\right) \tag{15}$$

Table 4 Calculated total and partial magnetic moments of CoFeTiGe and CoFeTiSb alloys

Alloy	Co	Magnetic moment (μ_B)				
		Fe	Ti	Ge/Sb	Interstitial	Total
CoFeTiGe						
mBJ	0.559	0.845	− 0.233	− 0.011	− 0.159	1.001
mBJ + SOC	0.697	0.775	− 0.243	− 0.020	− 0.210	0.998
Other work	0.55 [57]	0.69 [57]	− 0.23 [57]	− 0.01 [57]	–	1.00 [57]
	0.56 [51]	0.72 [51]	− 0.32 [51]	0.04 [51]	–	1.00 [51]
CoFeTiSb						
mBJ	1.172	1.431	− 0.336	0.001	− 0.267	2.001
mBJ + SOC	1.211	1.313	− 0.278	0.005	− 0.252	1.998
Other work	1.02 [58]	1.38 [58]	− 0.48 [58]	0.08 [58]	–	2 [58]

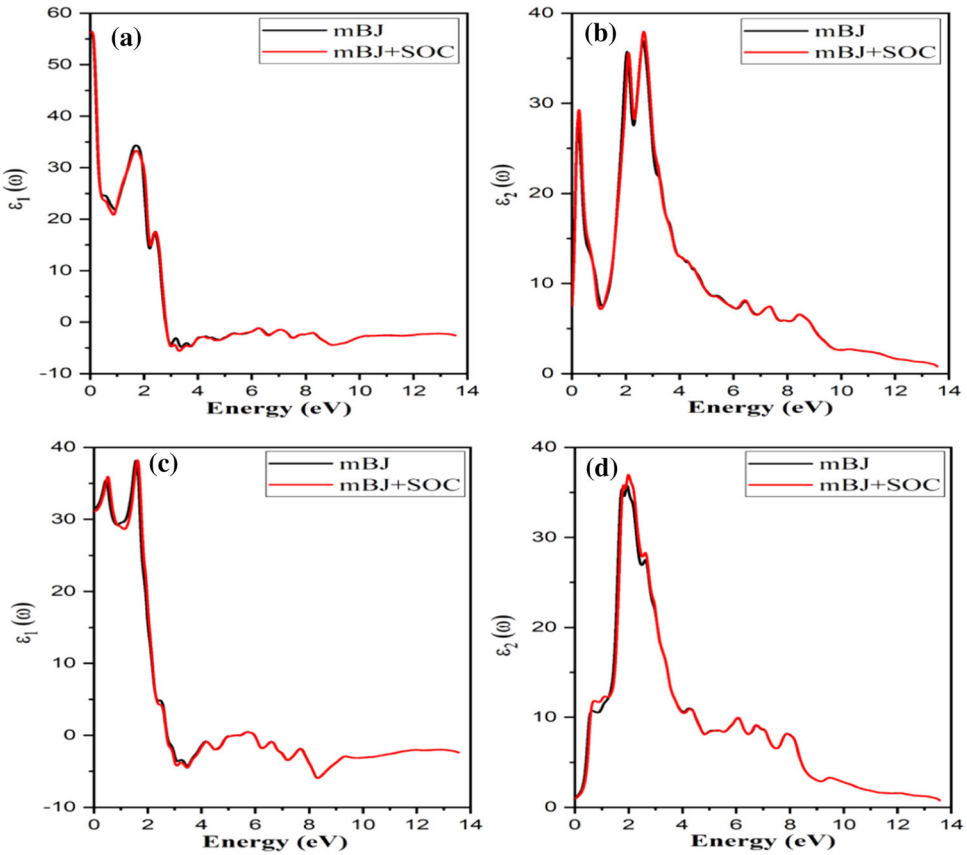

Fig. 6 The real and imaginary **a**, **b** of CoFeTiGe and real $\varepsilon_1(\omega)$, and imaginary **c**, **d** for CoFeTiSb with different potentials mBJ and mBJ + SOC

Here, the momentum operator is $\vec{p}$, the initial and final states are indicated with $\left|\vec{k}n\right\rangle$ and $\left|\vec{k}n'\right\rangle$, k, n, and n' are the wave vector and band index with corresponding energy of $E_{\vec{k}n}$ and $E_{\vec{k}n'}$, respectively. Also $f\left(\vec{k}n\right)$ and $f\left(\vec{k}n'\right)$ represent the Fermi Dirac distribution of initial and final states. The term $\delta\left(E_{\vec{k}n} - E_{\vec{k}n} - \hbar\omega\right)$ stands for the Dirac function. Kramers–Kronig relations present the possibility of arising the real part, which expresses as [62]:

$$\varepsilon_1 = 1 + \frac{2}{\pi}\int_0^{\infty} \frac{\varepsilon_2(\omega')\omega' d\omega'}{\omega'^2 - \omega'} \tag{16}$$

The real part $\varepsilon_1(\omega)$ helps to explain the dispersion of an electromagnetic wave while $\varepsilon_2(\omega)$ describes the energy loss in the medium. We also have calculated other significant optical parameters such as; reflectivity $R(\omega)$, refractive index $n(\omega)$, absorption coefficient $\sigma(\omega)$, and energy loss $L(\omega)$.

Real and imaginary parts of $\varepsilon(\omega)$ for both alloys are shown in Fig. 6 with mBJ and mBJ + SOC potentials. The selected energy range for both alloys is 0–14 eV. The $\varepsilon_1(\omega)$ have frequency-dependent spectra. At static point $\varepsilon_1(0)$, the dielectric constant values are 56.35 and 31.12 for CoFeTiGe and CoFeTiSb, respectively.

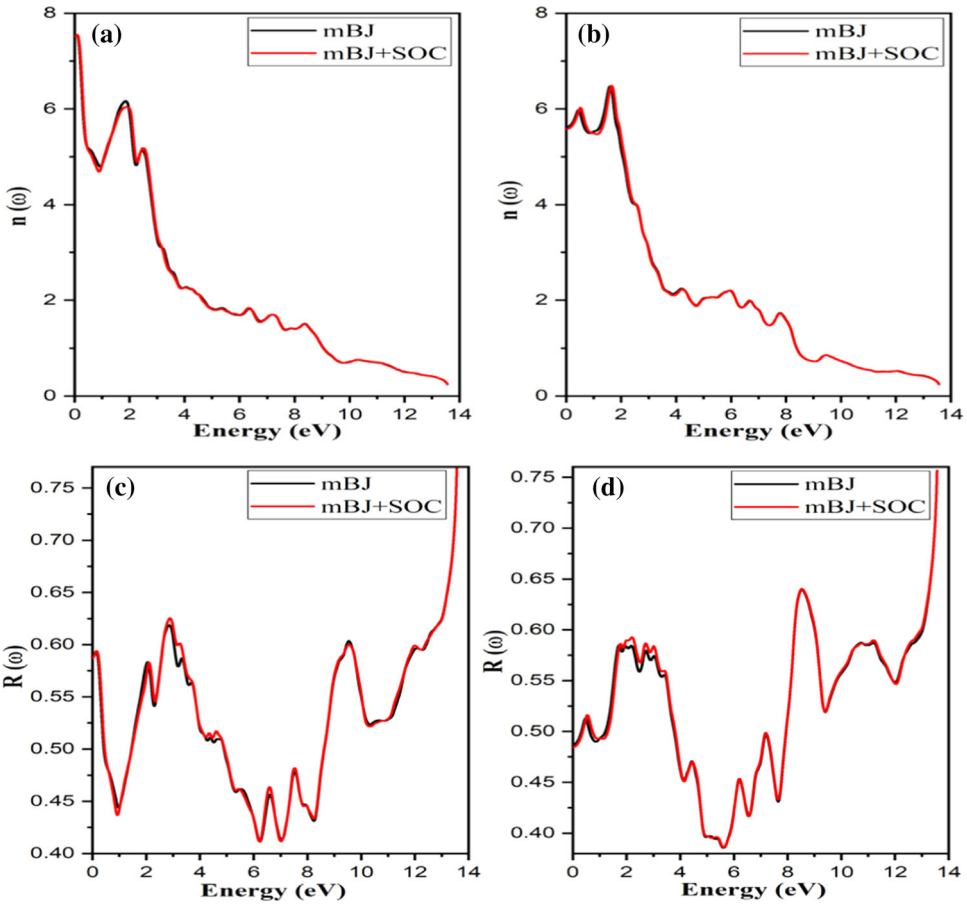

Fig. 7 Refractive index **a**, **b** and reflectivity **c**, **d** of CoFeTiZ (Z = Ge, Sb) alloys with mBJ and mBJ + SOC potentials

The maximum peak is observed at 1.72 and 1.70 eV for CoFeTiGe with mBJ and mBJ + SOC potentials, respectively. For CoFeTiSb, the first peak is observed at 0.44 eV with mBJ and 0.51 eV with mBJ + SOC while the maximum peak is seen at 1.56 eV with mBJ and 1.61 eV with mBJ + SOC potentials. These peaks appear due to the interband transition from the top most valance electrons to the bottom of the conduction band [63]. With further increase in energy, the peaks show a decreasing trend and reach the negative values at 2.8 eV for CoFeTiGe and 2.7 eV for CoFeTiSb. The $\varepsilon_2(\omega)$ explain the material's internal structure and absorptive nature. It is directly linked with the electronic band structure of the material. Figure 6b, d displays the imaginary part $\varepsilon_2(\omega)$ in the energy range of 0–14 eV. There are several peaks observed for CoFeTiGe alloy. The calculated peak values are 2.63 eV and 2.66 eV with mBJ and mBJ + SOC potentials, respectively. In the case of CoFeTiSb, the peak values are observed at 1.94 eV and 1.99 eV with mBJ and mBJ + SOC potentials, respectively. It can be seen that the peak values lie in the visible region for both alloys.

The calculated refractive index n (ω) of the selected alloys CoFeTiZ (Z = Ge, Sb) is illustrated in Fig. 7a, b. It is an important and dimensionless quantity that determines the transmission of light through the optical medium. The refractive index ($n(\omega) = (\omega) + ik$ (ω)) explains the refraction phenomenon, which plays an essential role in digital electronic devices such as solar cells, detectors, and photonic crystals. At static point, refractive index n(0) values are 7.53 and 7.51 for CoFeTiGe and 5.61 and 5.57 for CoFeTiSb with mBJ and mBJ + SOC potentials. Beyond zero frequency ($\omega = 0$), limit refractive index $n(\omega)$, increase and attain a maximum value at 1.85 eV and 1.89 eV for CoFeTiGe with mBJ and mBJ + SOC. For CoFeTiSb, the maximum values are achieved at 1.60 eV with mBJ and 1.65 eV with mBJ + SOC. The reflectivity of CoFeTiZ (Z = Ge, Sb) alloys as a function of photon energy is shown in Fig. 7c, d. Reflectivity is the ability of a material which measure the reflected light when incident on it. It is the ratio of the reflected wave energy at the surface to the incident wave energy at the surface [64]. At zero energy, reflectivity starts from 0.587 with mBJ and 0.586 with mBJ + SOC for CoFeTiGe and 0.486 with mBJ and 0.484 with mBJ + SOC for CoFeTiSb. There are several peaks observed in the visible and ultraviolet regions for both alloys. The evaluated optical conductivity profile for both alloys is demonstrated in Fig. 8a, b. It is a significant optical parameter that is an extension of electrical transport to optical frequency and is represented as:

$$\sigma(\omega) = \frac{2W_{\mathrm{CV}}\hbar\omega}{\vec{E}_0^2} \tag{17}$$

where W_{CV} is the transition probability per unit time [65]. The current density is generated when photons with absolute frequency are incident on the material, and this process is explained with the help of optical conductivity. The maximum optical conductivity

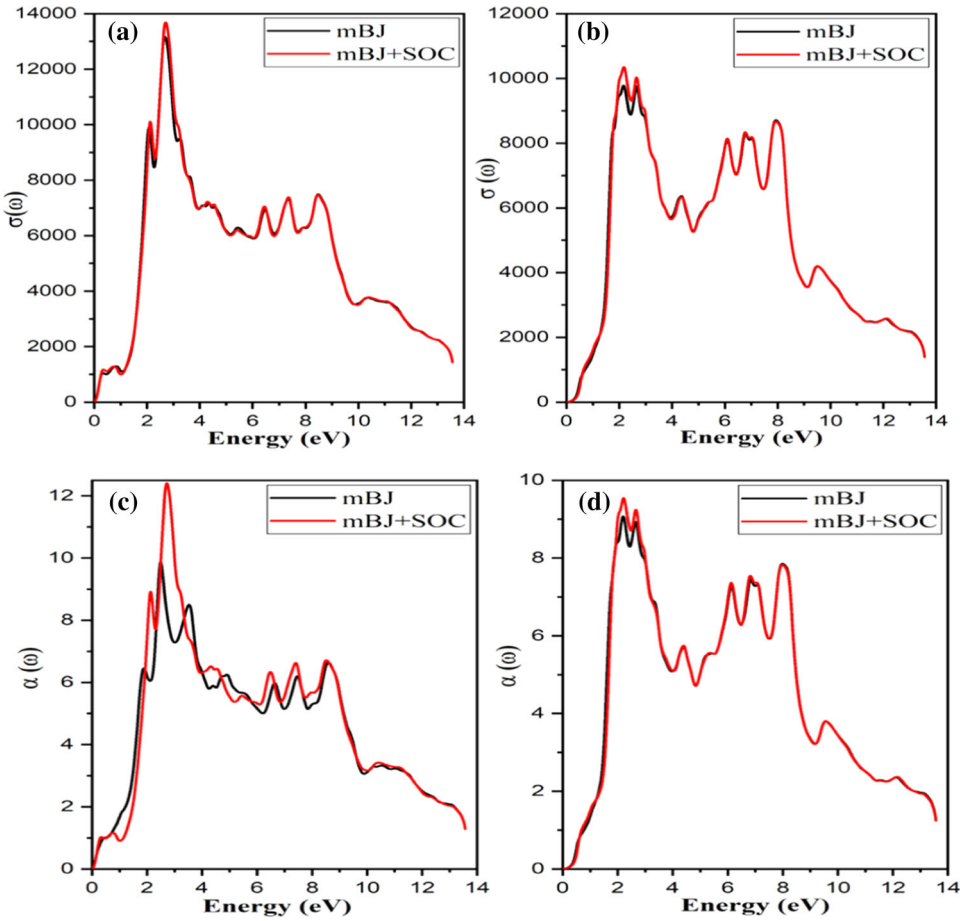

Fig. 8 The calculated optical conductivity (**a**, **b**) and absorption coefficient **c**, **d** for CoFeTiZ (Z = Ge, Sb) with mBJ, and mBJ + SOC potentials

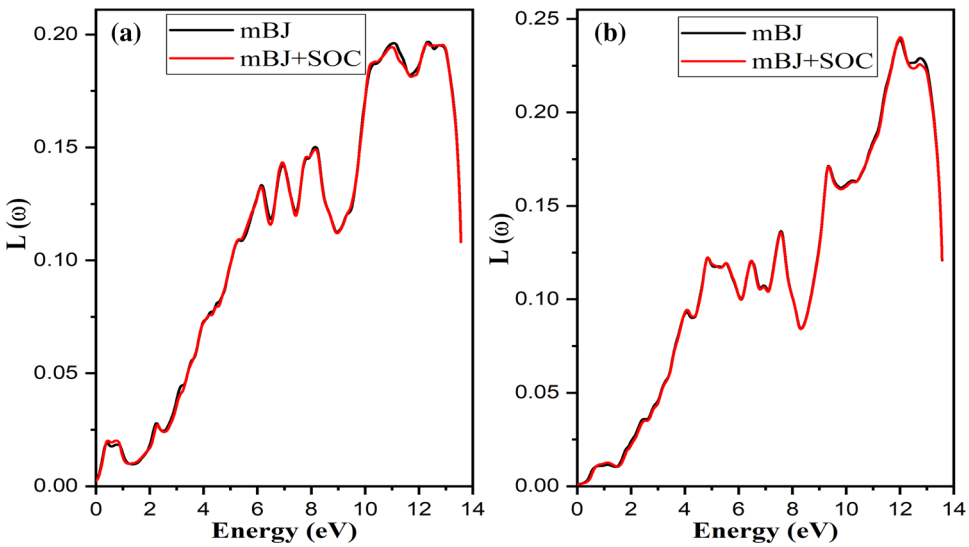

Fig. 9 The calculated energy loss function **a**, **b** of CoFeTiZ (Z = Ge, Sb) with mBJ, mBJ + SOC approximation

$\sigma(\omega)$ for the CoFeTiGe compound is 13165 at 2.66 eV with mBJ and 13,690 at 2.69 eV with mBJ + SOC potential. Furthermore, for the second alloy CoFeTiSb, the maximum optical conductivity is 9776 at 2.2 eV and 10,357 at 2.2 eV with mBJ and mBJ + SOC, respectively.

The ability of any material to absorb incident photons of specific energy ($E = \hbar\omega$) is directly related to its absorption coefficient $\alpha(\omega)$ [66]. The absorption coefficient $\alpha(\omega)$ also delivers data related to the optimum solar energy transformation efficiency. It provides evidence about the penetration of the specific energy light in the material before being absorbed. The absorption coefficient is zero when the light frequency is equal to the bandgap as shown in Fig. 8c, d. From the graphs, it is observed that both alloys

express similar behavior with very minor variations. The peak absorption values are observed at 2.45 eV with mBJ and 2.71 eV with mBJ + SOC for CoFeTiGe. In the case of CoFeTiSb, the maximum values are observed at 2.19 eV with mBJ and 2.23 eV with mBJ + SOC. The maximum absorption for both alloys occurred in the visible region, which shows their potential for optoelectronic devices. Furthermore, these alloys can also be used to absorb visible solar light for energy storage purposes in electronic devices.

Figure 9 personifies the optical loss function for CoFeTiZ (Z = Ge, Sb) alloys. The optical energy loss factor $L(\omega)$ measures the loss per unit area due to heating, plasma resonance, and scattering. It is a significant optical parameter that defines the utility of the materials against fast-moving electrons. Several peaks are observed in the calculated plots of both alloys. The minimum loss is seen in the visible region, which corresponds to the maximum absorption for both alloys.

7 Conclusion

We report the physical properties of quaternary Heusler alloys CoFeTiZ (Z = Ge, Sb) under the umbrella of density-functional theory employed via WIEN2k code. Our calculation shows that both structures are more stable in their ferromagnetic phase. A half-metallic nature is observed for both alloys, as depicted from the bandgap profile. The computed spin-polarized DOS illustrates a good agreement with the electronic band structure of the materials. The electron density plots predict the mixed bonding nature among the atoms in both alloys. The calculated total magnetic moments are 1.001 μ_β and 0.998 μ_β for CoFeTiGe and 2.001 μ_β and 1.998 μ_β for CoFeTiSb with mBJ and mBJ + SOC potentials, respectively. We have also investigated the optical behavior of the selected alloys by calculating the dielectric function, refractive index, optical conductivity, absorption, reflectivity and energy loss function. Maximum absorption and minimum energy loss are observed in the visible region for both alloys. The overall effect of SOC on the physical properties of both alloys is minimal because there is only a slight increase in the bandgap values with SOC. All calculated characteristics show that the studied quaternary Heusler alloys are potential candidates for various key applications such as energy storage and optoelectronics.

Data Availability Statement All data generated or analyzed during this study are included in this published article.

References

1. Y. Li et al., First-principles study on electronic structure, magnetism and half-metallicity of the NbCoCrAl and NbRhCrAl compounds. Results Phys. **7**, 2248–2254 (2017)
2. C. Felser, G.H. Fecher, B. Balke, Spintronics: a challenge for materials science and solid-state chemistry. Angew. Chem. Int. Ed. **46**(5), 668–699 (2007)
3. K. Inomata et al., Highly spin-polarized materials and devices for spintronics. Sci. Technol. Adv. Mater. **9**(1), 014101 (2008)
4. Y. Gao, X. Gao, The half-metallicity of LiMgPdSn-type quaternary Heusler alloys FeMnScZ (Z= Al, Ga, In): a first-principle study. AIP Adv. **5**(5), 057157 (2015)
5. S. Wolf et al., Spintronics: a spin-based electronics vision for the future. Science **294**(5546), 1488–1495 (2001)
6. Julliere M, Tunneling between ferromagnetic films. Phys. Lett. A **54**(3), 225–226 (1975)
7. S. Bahramian, F. Ahmadian, Half-metallicity and magnetism of quaternary Heusler compounds CoRuTiZ (Z= Si, Ge, and Sn). J. Magn. Magn. Mater. **424**, 122–129 (2017)
8. N.A. Koshi, R. John, Half-metallic ferrimagnetism in CoFeNbZ (Z= Al, Si, Ge, Sn) quaternary heusler alloys: a DFT study. J. Superconduct. Novel Magn. **32**(4), 977–986 (2019)
9. X.L. Wang, Proposal for a new class of materials: spin gapless semiconductors. Phys. Rev. Lett. **100**(15), 156404 (2008)
10. M.N. Rasool et al., Investigation of structural, electronic and magnetic properties of 1: 1: 1: 1 stoichiometric quaternary Heusler alloys YCoCrZ (Z= Si, Ge, Ga, Al): an ab-initio study. J. Magn. Magn. Mater. **395**, 97–108 (2015)
11. B. Pandey, R.B. Ray, G.C.J.B. Kaphle, First-principles study of structural, electronic and magnetic properties of Co-based quaternary Heusler compounds: CoFeCrAl, CoFeTiAs, CoFeCrGa and CoMnVAs. Bibechana **15**, 50–59 (2018)
12. M.H. Elahmar, H. Rached, D. Rached, The half metallic feature at high temperature of the novel half-Heusler alloys and their [100] oriented layered superlattices: a DFT investigations. Mater. Chem. Phys. **267**, 124712 (2021)
13. Ş Uğur et al., Elastic, mechanical, optical and magnetic properties of Ru2MnX (X= Nb, Ta, V) Heusler alloys. J. Magn. Magn. Mater. **523**, 167614 (2021)
14. J. Munir et al., Spin-polarized electromagnetic and optical response of full-Heusler Co2VZ (Z= Al, Be) alloys for spintronic application. Eur. Phys. J. Plus **136**(10), 1–18 (2021)
15. A. Taubel et al., Tailoring magnetocaloric effect in all-d-metal Ni-Co-Mn-Ti Heusler alloys: a combined experimental and theoretical study. Acta Mater. **201**, 425–434 (2020)
16. S. Mitra et al., Investigation on structural, electronic and magnetic properties of Co2FeGe Heusler alloy: experiment and theory. J. Magn. Magn. Mater. **552**, 169148 (2022)
17. D. Rani et al., Experimental and theoretical investigation on the possible half-metallic behaviour of equiatomic quaternary Heusler alloys: CoRuMnGe and CoRuVZ (Z= Al, Ga). J. Magn. Magn. Mater. **492**, 165662 (2019)
18. L. Bainsla et al., High spin polarization in CoFeMnGe equiatomic quaternary Heusler alloy. J. Appl. Phys. **116**(20), 203902 (2014)
19. L. Bainsla et al., High spin polarization and spin splitting in equiatomic quaternary CoFeCrAl Heusler alloy. J. Magn. Magn. Mater. **394**, 82–86 (2015)
20. L. Bainsla et al., Spin gapless semiconducting behavior in equiatomic quaternary CoFeMnSi Heusler alloy. Phys. Rev. B **91**(10), 104408 (2015)
21. L. Bainsla et al., Origin of spin gapless semiconductor behavior in CoFeCrGa: theory and experiment. Phys. Rev. B **92**(4), 045201 (2015)
22. S. Berri, First-principles study on half-metallic properties of the CoMnCrSb quaternary Heusler compound. J. Superconduct. Novel Magn. **29**(5), 1309–1315 (2016)

23. M. Elahmar et al., Structural, mechanical, electronic and magnetic properties of a new series of quaternary Heusler alloys CoFeMnZ (Z= Si, As, Sb): a first-principle study. J. Magn. Magn. Mater. **393**, 165–174 (2015)
24. P. Klaer et al., Element-specific magnetic moments and spin-resolved density of states in CoFeMn Z (Z= Al, Ga; Si, Ge). Phys. Rev. B **84**(14), 144413 (2011)
25. A. Bahnes et al., Half-metallic ferromagnets behavior of a new quaternary Heusler alloys CoFeCrZ (Z= P, As and Sb): Ab-initio study. J. Alloys Compd. **731**, 1208–1213 (2018)
26. K. Benkaddour et al., First-principles study of structural, elastic, thermodynamic, electronic and magnetic properties for the quaternary Heusler alloys CoRuFeZ (Z= Si, Ge, Sn). J. Alloys Compd. **687**, 211–220 (2016)
27. M. Benkabou et al., Electronic structure and magnetic properties of quaternary Heusler alloys CoRhMnZ (Z= Al, Ga, Ge and Si) via first-principle calculations. J. Alloys Compd. **647**, 276–286 (2015)
28. Y. Zhang et al., Influence of order on the magnetic and electronic properties of quaternary half-metallic Heusler CoFeTiSn alloy. J. Alloy. Compd. **842**, 155977 (2020)
29. Y. Zhang et al., Structural, electronic and magnetic properties of CoFeTiGa1−xSbx compounds. J. Magn. Magn. Mater. **422**, 32–36 (2017)
30. X.Q. Chen, R. Podloucky, P. Rogl, Ab initio prediction of half-metallic properties for the ferromagnetic Heusler alloys Co 2 M Si (M= Ti, V, Cr). J. Appl. Phys. **100**(11), 113901 (2006)
31. K. Özdog et al., Defects-driven appearance of half-metallic ferrimagnetism in Co–Mn-based Heusler alloys. Solid State Commun. **142**(9), 492–497 (2007)
32. H.C. Kandpal, G.H. Fecher, C. Felser, Calculated electronic and magnetic properties of the half-metallic, transition metal based Heusler compounds. J. Phys. D Appl. Phys. **40**(6), 1507 (2007)
33. G. Liu et al., Mn 2 co z (z= al, ga, in, si, ge, sn, sb) compounds: Structural, electronic, and magnetic properties. Phys. Rev. B **77**(1), 014424 (2008)
34. K. Özdog, I. Galanakis, First-principles electronic and magnetic properties of the half-metallic antiferromagnet Cr2MnSb. J. Magnet. Magn. Mater. **321**(15), L34–L36 (2009)
35. V. Sharma et al., Electronic, magnetic and transport properties of Co2TiZ (Z= Si, Ge and Sn): A first-principle study. J. Magn. Magn. Mater. **322**(19), 2922–2928 (2010)
36. H. Mori et al., Electronic band structure calculations on thin films of the L21 full Heusler alloys X2YSi (X, Y= Mn, Fe, and Co): Toward spintronic materials. Thin Solid Films **520**(15), 4979–4983 (2012)
37. P. Blaha, et al., WIEN2k. in *An Augmented Plane Wave + Local Orbitals Program for Calculating Crystal Properties* (Karlheinz Schwarz, Techn. Universitat Wien, Austria, 2001). ISBN 3-9501031-1-2
38. H. Dixit et al., Electronic structure of transparent oxides with the Tran-Blaha modified Becke-Johnson potential. J. Phys.: Cond. Matter **24**(20), 205503 (2012)
39. S. Tariq et al., Ab initio study on half-metallic, electronic and thermodynamic attributes of LaFeO3. Eur. Phys. J. Plus **133**(3), 1–10 (2018)
40. F. Tran, P. Blaha, Accurate band gaps of semiconductors and insulators with a semilocal exchange-correlation potential. Phys. Rev. Lett. **102**(22), 226401 (2009)
41. D. Koelling, B.N. Harmon, A technique for relativistic spin-polarised calculations. J. Phys. C: Solid State Phys. **10**(16), 3107 (1977)
42. F. Birch, Finite elastic strain of cubic crystals. Phys. Rev. **71**(11), 809 (1947)
43. G. Wang et al., Broadband and ultra-thin terahertz metamaterial absorber based on multi-circular patches. Eur. Phys. J. **86**(7), 1–9 (2013)
44. M. Shakil et al., Theoretical investigation of structural, magnetic and elastic properties of half Heusler LiCrZ (Z= P, As, Bi, Sb) alloys. Phys. B Condens. Matter **575**, 411677 (2019)
45. H. Fu et al., Ab initio calculations of elastic constants and thermodynamic properties of NiAl under high pressures. Comput. Mater. Sci. **44**(2), 774–778 (2008)
46. K. Yao et al., Half-metallic ferromagnetism of zinc-blende CrS and CrP: a first-principles pseudopotential study. Solid State Commun. **133**(5), 301–304 (2005)
47. G. Gao et al., Half-metallic ferromagnetism in zinc-blende CaC, SrC, and BaC from first principles. Phys. Rev. B **75**(17), 174442 (2007)
48. B. Fadila et al., Structural, magnetic, electronic and mechanical properties of full-Heusler alloys Co2YAl (Y= Fe, Ti): first principles calculations with different exchange-correlation potentials. J. Magn. Magn. Mater. **448**, 208–220 (2018)
49. D. Bensaid et al., First-principle investigation of structural, electronic and magnetic properties in Mn 2 RhZ (Z= Si, Ge, and Sn) Heusler alloys. J. Superconduct. Novel Magn. **29**(7), 1843–1850 (2016)
50. R. Haleoot, B. Hamad, Thermodynamic and thermoelectric properties of CoFeYGe (Y= Ti, Cr) quaternary Heusler alloys: first principle calculations. J. Phys.: Condens. Matter **32**(7), 075402 (2019)
51. Y. Zhang et al., Magnetism, band gap and stability of half-metallic property for the quaternary Heusler alloys CoFeTiZ (Z= Si, Ge, Sn). J. Alloy. Compd. **616**, 449–453 (2014)
52. Z. Charifi, et al., Characterization of quaternary Heusler alloys CoFeYGe (Y = Ti, Cr) with respect to structural, electronic, magnetic, mechanical, and thermoelectric features. Int. J. Energy Res. **46**(10), 13855–13873 (2022). https://doi.org/10.1002/er.8104
53. L. Xiong, L. Yi, G. Gao, Search for half-metallic magnets with large half-metallic gaps in the quaternary Heusler alloys CoFeTiZ and CoFeVZ (Z= Al, Ga, Si, Ge, As, Sb). J. Magn. Magn. Mater. **360**, 98–103 (2014)
54. S. Berri et al., A first-principle study of half-metallic ferrimagnetism in the CoFeTiSb quaternary Heusler compound. J. Magn. Magn. Mater. **354**, 65–69 (2014)
55. Z. Liu et al., Role of dd and pd hybridization in CoTi-based magnetic semiconductors with 21 and 26 valence electrons. J. Phys. D Appl. Phys. **48**(32), 325001 (2015)
56. I. Galanakis, P. Dederichs, N. Papanikolaou, Slater-Pauling behavior and origin of the half-metallicity of the full-Heusler alloys. Phys. Rev. B **66**(17), 174429 (2002)
57. R. Haleoot, B. Hamad, Thermodynamic and thermoelectric properties of CoFeYGe (Y= Ti, Cr) quaternary Heusler alloys: first principle calculations. J. Phys.: Condens. Matter **32**(7), 075402 (2019)
58. Z. Liu et al., Role of dd and pd hybridization in CoTi-based magnetic semiconductors with 21 and 26 valence electrons. J. Phys. D: Appl. Phys. **48**(32), 325001 (2015)
59. H. Zhu et al., Electronic structures and optical properties of rutile TiO2 with different point defects from DFT+ U calculations. Phys. Lett. A **378**(36), 2719–2724 (2014)
60. A. Bakar et al., Optoelectronic Properties of CuCoMnZ (Z= Si, Sn, Sb): A DFT Study. J. Electron. Mater. **50**(7), 4006–4015 (2021)
61. C. Ambrosch-Draxl, J.O. Sofo, Linear optical properties of solids within the full-potential linearized augmented planewave method. Comput. Phys. Commun. **175**(1), 1–14 (2006)
62. J.S. Toll, Causality and the dispersion relation: logical foundations. Phys. Rev. **104**(6), 1760 (1956)

63. S. Thahirunnisa, I.B. Banu, Optical properties of novel ASiP 2 (A= Ca, Sr) chalcopyrites: first-principle study. Appl. Phys. A **124**(12), 1–7 (2018)
64. M. Hadi et al., Mechanical behaviors, lattice thermal conductivity and vibrational properties of a new MAX phase Lu2SnC. J. Phys. Chem. Solids **129**, 162–171 (2019)
65. G. Murtaza, I. Ahmad, First principle study of the structural and optoelectronic properties of cubic perovskites CsPbM3 (M= Cl, Br, I). Phys. B: Condens. Matter **406**(17), 3222–3229 (2011)
66. M. Hilal et al., Investigation of electro-optical properties of InSb under the influence of spin-orbit interaction at room temperature. Mater. Chem. Phys. **184**, 41–48 (2016)